

Statistical topology optimization scheme for structural damage identification

Kyobeom Ku^a, Kamilla E.S. Silva^b, Gil Ho Yoon^{a,1}

^a School of Mechanical Engineering, Hanyang University, Seoul, South Korea

^b Department of Naval Architecture and Ocean Engineering, Polytechnic School, University of São Paulo, São Paulo, Brazil

ARTICLE INFO

Article history:

Received 6 December 2022

Accepted 30 May 2023

Available online 16 June 2023

Keywords:

Topology optimization

Damage identification

Statistical analysis

Clustering

ABSTRACT

Statistical topology optimization (TO) scheme, which statistically records and analyzes local optima at random frequencies of the excitation force, is developed for material damage and open crack. To identify the alternations of stiffness, mass, and strength due to the damages, the structural responses of healthy and suspicious systems can be compared and optimized by TO for fault identification. Owing to the local optima problem in TO, slight modifications in responses caused by relatively minimal damage, and inadequate comparison of insufficient vibration information, the application of TO to a damage identification problem is often complicated. To overcome this complication, this study establishes a new approach that records local optima (layouts) and performs a statistical process (clustering and averaging of layouts). To illustrate the concept of the present scheme, several examples with material damage and open crack are solved.

© 2023 Published by Elsevier Ltd.

1. Introduction

In this study, a statistical topology optimization (STO) scheme, which statistically records and analyzes layouts that are locally optimized at several randomly selected frequencies, is developed to improve the accuracy of structural damage identification. As structural damage and cracking are known to modify the mechanical properties of structures including the stiffness, mass, and damping characteristics, the responses of healthy and suspicious systems can be compared for fault identification [1–5]. In particular, structural topology optimization (TO) can be adapted to identify damage [6–11]. Although this concept and approach are important engineering methods, certain limitations exist. First, the frequency ranges of frequency response functions (FRFs) are defined based on damage characteristics including the damage type and the size and shape of the damage area. Therefore, without knowledge of the damage characteristics, selecting a frequency range for damage identification based on a comparison of FRFs is a theoretically recursive problem. In addition, the identification process frequently fails owing to the local optima problem of TO encountered in recovering the frequency responses of a damaged structure. To alleviate these difficulties, this study develops a new scheme that records local optima and performs a statistical

process (clustering and averaging). Several numerical examples reveal that the local optima of the existing TO scheme can be divided into a cluster and outliers. Consequently, several local optima around a global optimum can be clustered to identify a damaged structure.

Several relevant studies have been conducted on structural damage identification, localization, and characterization using the FRFs [12–18]. A literature review of such damage identification methods is, however, beyond the scope of the present study. Detailed information on the same can be found elsewhere [19–21]. However, briefly, these studies aimed to identify damage by analyzing and comparing FRFs. In [12,13], an FRF curvature method based on measured data without any modal identification was presented. In [14–16], artificial neural networks were applied to identify damage using FRFs. Recently, several deep learning methods have been developed for damage identification (see [17,18] and the references therein). To obtain more detailed information on the damage state, a mathematical model and the measured responses of structures can be combined [22–25]. An optimization scheme can also be used to mathematically update the parameters of a system model. Global optimization algorithms, including genetic algorithms and particle swarm optimization algorithms, are utilized with model-based structural damage identification approaches to avoid local optima issue [26–30]. In [28], a genetic algorithm was used to identify structural damage by comparing differences in structural static displacements. In [29], a genetic

¹ Department of Mechanical Engineering, College of Engineering, Hanyang University, Seoul, South Korea.

E-mail address: ghy@hanyang.ac.kr (G.H. Yoon)

algorithm and simulated annealing algorithm were combined to enhance the damage identification performance by comparing both static and dynamic responses of structures. However, above studies have only been successful with FE models consisting of a small number of elements due to the numerous computational time caused by the slow convergence rate of the algorithms. Some studies utilizing the concept of TO can be found in [6–11]. In [6], a TO formulation considering both resonances and anti-resonances for structural damage identification was presented, and a progressive design variable reduction strategy, which gradually reduced the candidates of damaged elements at each stage, was developed. To our best knowledge, this research is the pioneer research for the damage identification by TO. In [7], as an extension of the study presented in [6], damage caused to composite beams was identified based on experimental vibration test data. In [8], a modal-based damage identification method was demonstrated to improve the identification accuracy by further considering or optimizing eigenmodes, as well as eigenvalues in case the eigenmodes of damaged and intact structures differed. Furthermore, several studies have demonstrated that increasing the amount of information can enhance the accuracy of damage identification [9–11,31]. In [9,10], a new damage identification method that combined TO and ultrasonic wave propagation was presented. The accuracy of damage identification was increased by using data set of ultrasonic propagation incidents from multiple directions. In [11], full-field response data were obtained using digital image correlation in a TO framework to locate and qualify structural damage. The accuracy of damage identification was improved by increasing the number of sensing points. In [31], a void identification method using level set method and transient response of structures was presented and enhanced the identification accuracy by increasing the number of measuring points. As an extension of these contributions, this research illustrates the limitation of the conventional TO (CTO) scheme in minimizing the difference between measured and model FRFs and develops an STO scheme.

The present study also attempts to identify structural damage using TO with FRFs, as presented in Fig. 1(a). Specifically, the two types of damage, i.e., material damage and an open crack, are considered as illustrated in Fig. 1(c). The Young's modulus and mass density values of damaged finite elements are assumed to be altered to model the first damage type or material damage. For the second damage type, the element connectivity parameterization method (ECP) is used to represent structural cracks [32]. Artificial links connect each finite element and disconnect adjacent elements according to link stiffness values for modeling cracks in structures. Although diagonal links complicate optimization problems by increasing the number of design variables, all adjacent nodes of elements are connected to model the actual structure similarly in this study. In our implementation, several local optima are obtained depending on the selected frequencies, as presented in Fig. 1(b); however, we believe that it is often extremely difficult to identify damage by interpreting optimized layouts. To overcome this issue, a statistical method is established. Particularly, considering that several local optima depend on the frequency or the frequency domain of interest, which is a fixed parameter in the CTO, numerous local optima are statistically processed with a set of randomly chosen frequencies. Note that a global optimum does not vary according to the selected frequencies; therefore, this study assumes that similar local optima demonstrate a high probability of being near the true solution. Thus, implementing several TO processes with random frequency points and clustering optimized layouts, increases the probability of identifying a damaged model. Among the several presented clustering algorithms, the density-based spatial clustering of applications with noise (DBSCAN) algorithm [33] is adopted. Using the structural TO method, several local optima in certain specified frequency ranges are obtained and

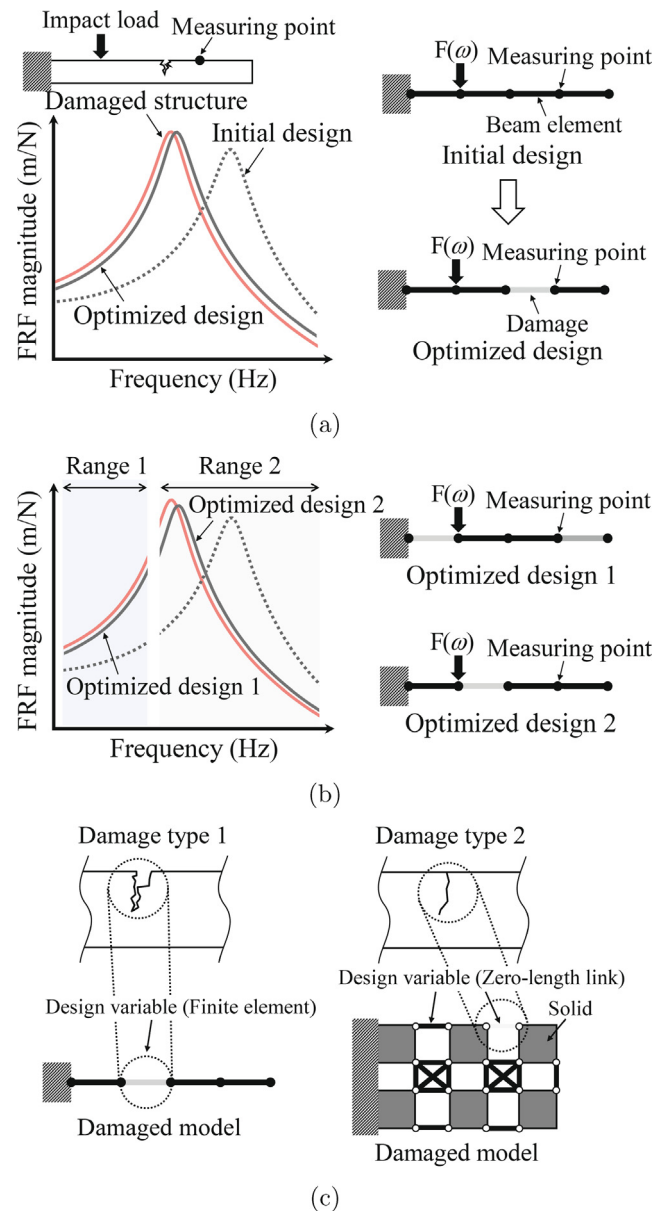


Fig. 1. Topology optimization for structural damage identification based on a frequency response function. (a) Topology optimization with frequency or frequency domain of interest, (b) local optima issue depending on the frequency domain, and (c) parameterization strategies for each damage type.

statistically analyzed using the DBSCAN algorithm for clustering in damage identification.

The remainder of this paper is organized as follows. Section 2 describes the development of the STO scheme with TO formulation and cluster analysis. Section 3 presents the application of the presented method to several damage identification problems and compares the obtained results with those derived using the CTO. Finally, conclusions and suggestions for future research are provided in Section 4.

2. Statistical topology optimization

This section describes the development of the STO scheme, which is illustrated in Fig. 2. This scheme records and analyzes topologically optimized layouts to overcome the following limitations of structural damage identification using a TO scheme: local

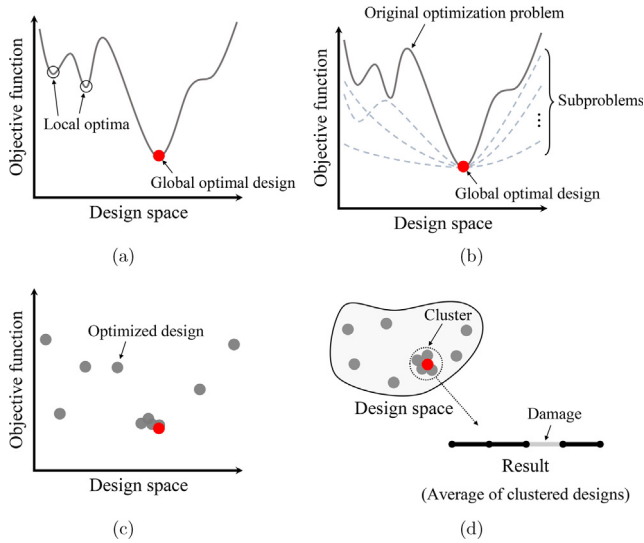


Fig. 2. Conceptual scheme of statistical topology optimization. (a) Optimization problem with two local optima marked as black circles and one global optimum depicted as a red circle (design space: solution space of the optimization problem), (b) the conceptual function space of the original optimization problem and subproblems (dotted lines), (c) distribution of local optima, and (d) cluster analysis of the optimized designs.

optima problem, small changes in responses, and insufficient information. The purpose of the developed STO scheme is to obtain a finite element (FE) model with healthy and damaged elements possessing the same or a similar frequency response as that of the corresponding damaged structure by solving several optimization problems and performing statistical analysis (clustering and averaging). After the FRFs of the damaged structure are obtained, a numerical integration of the difference between the FRFs of the damaged structure and those of the FE model of the intact structure is set as the objective function to be minimized. However, owing to the complexity of the FRFs in terms of the resonance peak(s), anti-resonance(s), and frequency domains, an optimization problem with an integration of the above difference frequently yields a local optimum, as presented in Fig. 2(a) [34]. In particular, because the CTO scheme based on the solid isotropic material with penalization method [35] commonly adopts a gradient-based optimizer, a global optimal design representing the locations and severity of actual damage is difficult to obtain.

Therefore, this study emphasizes that the original TO problem (see Eq. (7) based on the difference between FRFs) can be modified and reformulated to generate several optima from a statistical perspective. Specifically, several sub TO problems with different frequency domains, as expressed in Eq. (7), can be solved, and the results, i.e., the layouts obtained from the sub TO problems, are *statistically clustered*. This problem solving considers that a global optimum (the FE model with phenomenological damage) exists uniquely regardless of the choice of the *frequency domain* and the optimization problem. This is illustrated in Fig. 2(b). Here, it is assumed that the boundary conditions of the force and displacement are precisely known to engineers in advance. Notably, several numerical factors (such as the initial design variables, optimization algorithms, and convergence criteria) and several theoretical aspects (such as optimization and FE formulations) cause the optima of the subproblems to differ. However, the frequency domain considered while calculating the FRFs is varied within the same optimization formulation for numerical simplicity. A statistically meaningful dataset can also be obtained by perturbing other different conditions with the ambiguity of a statistically meaningful dataset as presented in Fig. 2(c). However, local optima

having objective function values similar to that of the global solution but far from the true solution can be obtained as shown in Fig. 2(c). Therefore, it is difficult to select an appropriate optimized design among obtained solutions only based on their objective function values. A clustering algorithm, here the DBSCAN algorithm [33], is used to identify the similarities and differences among the obtained layouts and divide them into a cluster and outliers as shown in Fig. 2(d). This study emphasizes that averaging the clustered layouts demonstrates a high probability of obtaining a global optimum, as shown in Fig. 2(d), considering that only a single global optimal design with damage exists. The STO algorithm explained above is depicted in Fig. 2. The three steps in Fig. 2(b)–(d) are repeated until the layout (average of the clustered designs) converges; an explanation of the convergence criterion can be found elsewhere [36].

2.1. Topology optimization formulation for damage identification

Finite element analysis

In the present method, the optimized designs are collected via repeated TO and analyzed to identify structural damage. In this subsection, the formulation of the TO method for damage identification is presented.

The dynamic behavior of a structure in frequency domain is expressed as

$$\mathbf{S}(\omega)\mathbf{X}(\omega) = \mathbf{F}(\omega) \quad (1)$$

$$\mathbf{S}(\omega) = -\omega^2\mathbf{M} + i\omega\mathbf{C} + \mathbf{K} \quad (2)$$

where \mathbf{X} and \mathbf{F} denote the displacement and exciting force vectors at the angular velocity, ω , respectively. The mass, Rayleigh damping, and stiffness matrices are denoted as \mathbf{M} , \mathbf{C} , and \mathbf{K} , respectively. For simplicity, the Rayleigh damping, $\mathbf{C} = \alpha\mathbf{M} + \beta\mathbf{K}$, is assumed with proportional constants α and β . The dynamic stiffness matrix is denoted as \mathbf{S} . Each element at the (i,j) -th position in the inverse matrix of the dynamic stiffness matrix, \mathbf{S}^{-1} , reflects the FRF between the j -th single input and the i -th single output. Moreover, each element at the i -th position of the displacement vector, \mathbf{X} , represents a single-output FRF for a single input or multiple inputs depending on the condition of the excitation vector, \mathbf{F} . Therefore, \mathbf{X} , which represents the broader form of an FRF, is utilized for damage identification.

Models of Material damage and open crack

This study considered the two damage types using two parameterization strategies as shown in Fig. 2(c). For the damage type 1 (Material damage), the Young's modulus and structural density values of each element are interpolated as follows²:

$$E_e = \gamma_e^3 E_0, \quad \rho_e = \gamma_e \rho_0 \quad (3)$$

where E_0 and ρ_0 denote the nominal Young's modulus and the structural density, respectively, and γ_e is the design variable of the e -th element in the FE model. In order to address the damage type 2 (open crack) in two-dimensional space, the stiffness values of each zero-length links are parameterized as follows:

$$l_e = \gamma_e^3 l_0 \quad (4)$$

² A critical assumption of material modeling is that structural damage decreases the Young's modulus with a polynomial of power 3 and that the element density varies linearly with the element design variable. As the present research is to establish an STO concept, the material modeling method presented in [6–8] is employed.

$$\mathbf{k}_e^{\text{link}} = l_e \mathbf{k}_{\text{nominal}}^{\text{link}} = l_e \begin{bmatrix} 1 & 0 & -1 & 0 \\ 0 & 1 & 0 & -1 \\ -1 & 0 & 1 & 0 \\ 0 & -1 & 0 & 1 \end{bmatrix} \quad (5)$$

where l_e and l_0 indicate the stiffness of the e -th link and upper bound of an elastic link representing elements connectivity, respectively. The e -th link element stiffness and the nominal stiffness are denoted by $\mathbf{k}_e^{\text{link}}$ and $\mathbf{k}_{\text{nominal}}^{\text{link}}$, respectively. The value of l_0 is set to 10^3 times the first diagonal stiffness element of an adjacent finite element (See details in [32]).

Error measure and optimization formulation

The summation of errors at discrete frequencies between the magnitudes of the responses of a damaged structure, $|X_k^*(\omega_j)|$, and those of a guessed, imagined, or optimized structure, $|X_k(\omega_j)|$, is defined as *FRFError*, as follows:

$$\text{FRFError} = \sum_{j=1}^{N_\omega} \sum_{k=1}^{N_m} \left(\frac{|X_k^*(\omega_j)| - |X_k(\omega_j)|}{|X_k^*(\omega_j)|} \right)^2 \quad (6)$$

where the number of selected frequency points at which the responses are obtained and the number of measuring points are denoted as N_ω and N_m , respectively. The frequency-dependent responses of the damaged model and optimized structure are denoted by X_k^* and X_k , respectively. Note that without normalizing the responses of the damaged structure, a large value of $(|X_k^*(\omega_j)| - |X_k(\omega_j)|)$ underestimates the meaningful differences at other sampling frequencies. Because data pertaining to the system are proportional to the number of measuring points, considering several measuring points may be helpful. However, the selection of *appropriate* measuring points is also challenging from an engineering perspective. In several previous studies [37–39], single- or multi-objective optimization problems that maximize the obtained information (e.g., vibration, strain, and wave propagation) have been solved for the selection of measuring points. Furthermore, the selection of the frequency range significantly affects the accuracy of damage identification using FRFs. If any engineering scheme tailored to estimate damage provides structures with zero *FRFError*, the probability of successfully identifying and estimating characteristics such as the size, shape, and topology of the existing damage is high. To achieve this effectively, several engineering approaches have been developed so far [23–25].

The TO problem is formulated as follows:

$$\begin{aligned} \underset{\gamma}{\text{minimize}} \quad & \Phi(\gamma, \omega) = \sum_{j=1}^{N_\omega} \sum_{k=1}^{N_m} \left(1 - \frac{|X_k(\omega_j)|}{|X_k^*(\omega_j)|} \right)^2 \\ & + \lambda \sum_{e=1}^{N_e} (1 - \gamma_e), \\ \text{subject to} \quad & \mathbf{S}\mathbf{X} = \mathbf{F}, \bar{\mathbf{S}}\bar{\mathbf{X}} = \bar{\mathbf{F}} \\ & 0 < 0.001 = \gamma_{\min} \leq \gamma_e \leq 1 \\ & (e = 1, 2, \dots, N_e), \end{aligned} \quad (7)$$

where γ and ω denote the design variable vector and the set of selected frequency points, respectively. The coefficient of the penalty term (the second term of the objective function) and the number of elements are denoted by λ and N_e , respectively. The overbar of the system matrix or the vector indicates a complex conjugation. The objective function, Φ , consists of two terms: *FRFError* and penalty. The physical relevance of the above optimization problem is to determine the distributions of the spatially varying design variables to render the FRFs of the optimized model identical to the obtained FRFs of the damaged model. The penalty term, $\lambda \sum_{e=1}^{N_e} (1 - \gamma_e)$, is added assuming that the number of damaged FEs is smaller than that of intact domains. This allows the design variables of

the elements without damage become close to one. The coefficient, λ , of the penalty term is updated as the absolute value of the median of the sensitivity vector in the *FRFError* term every 20 iterations to ensure that the value of the penalty term is not greater than the value of *FRFError* during optimization. The objective function, Φ , can be differentiated with respect to the design variable, γ_e , as follows:

$$\frac{\partial \Phi}{\partial \gamma_e} = (-2) \sum_{j=1}^{N_\omega} \sum_{k=1}^{N_m} \left(\frac{|X_k^*(\omega_j)| - |X_k(\omega_j)|}{|X_k^*(\omega_j)|^2} \right) \cdot \frac{\partial |X_k(\omega_j)|}{\partial \gamma_e} - \lambda \quad (8)$$

The term, $\frac{\partial |X_k(\omega_j)|}{\partial \gamma_e}$, which denotes the sensitivity of the FRF magnitude at the k -th measurement point, can be expressed as

$$\frac{\partial |X_k(\omega_j)|}{\partial \gamma_e} = \frac{1}{2|X_k(\omega_j)|} \left(\frac{\partial X_k(\omega_j)}{\partial \gamma_e} \bar{X}_k(\omega_j) + X_k(\omega_j) \frac{\partial \bar{X}_k(\omega_j)}{\partial \gamma_e} \right) \quad (9)$$

To derive the sensitivity of the FRF at the k -th measurement point $\frac{\partial X_k}{\partial \gamma_e}$ and its conjugate value $\frac{\partial \bar{X}_k}{\partial \gamma_e}$ in Eq. (9), both sides of Eq. (1) can be differentiated. Moreover, the sensitivity vector of this FRF can be expressed as

$$\frac{\partial \mathbf{X}}{\partial \gamma_e} = \mathbf{S}^{-1} \left(-\frac{\partial \mathbf{S}}{\partial \gamma_e} \mathbf{X} \right) \quad (10)$$

The sensitivity of the FRF at the k -th measurement point can be expressed as

$$\frac{\partial X_k}{\partial \gamma_e} = \mathbf{L}_k \frac{\partial \mathbf{X}}{\partial \gamma_e} \quad (11)$$

where \mathbf{L}_k is a row vector wherein only the value of the component corresponding to the degrees of freedom of the k -th measurement point is 1, and the remaining values are 0. The above optimization formulation and sensitivity analysis aim to identify damage in the TO framework [40,24].

2.2. Cluster analysis

Clustering classifies and groups objects based on their similarities. Clustering is an important tool in data analysis, and several clustering algorithms have been developed (see [41,42] and references therein). Clustering algorithms can be classified into centroid-based algorithms such as k -means clustering and CLARANS and density-based algorithms such as DBSCAN and OPTICS [33,43]. Centroid-based algorithms have the disadvantages of requiring an input parameter for the number of clusters, finding non-convex clusters, and being weak to data set with outliers [43,44]. On the other hand, density-based algorithms can identify outliers that lie in low-density regions and create clusters of arbitrary shapes. In the STO scheme, there is no prior information on the distribution of collected local optima, and outliers, designs far from a global solution, can be obtained. Thus, DBSCAN, one of the most famous density-based clustering method, is adopted in this study. The data, i.e., the optimized layouts, are clustered using the DBSCAN algorithm, as presented in Fig. 3. This algorithm analyzes the distance between points in a dataset, creates clusters of points (core and border points), and considers other points in a low-density region as outliers.

In the present study, DBSCAN parameters are chosen to obtain only *one* cluster, which exhibits the highest probability for correct damage identification. The choice of a single cluster is made because we aim to identify a damaged structure that is physically in existence. Algorithm 1 presents the simplified pseudocode of the algorithm for DBSCAN parameters selection. Setting a small *eps*

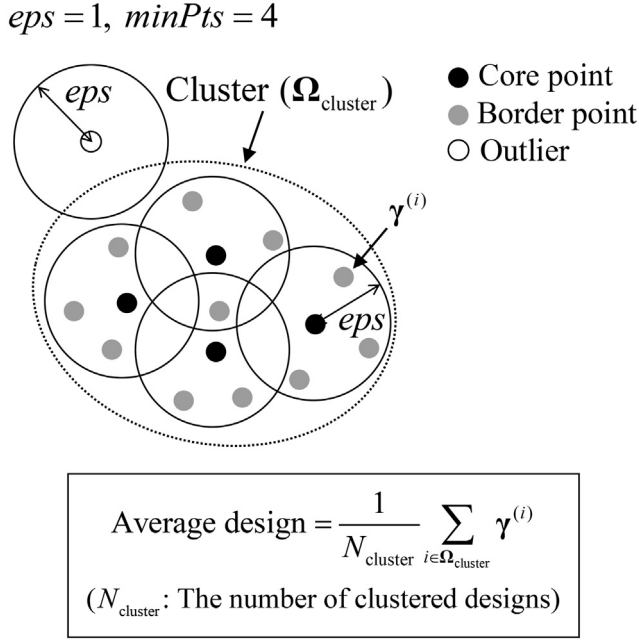


Fig. 3. Concept of DBSCAN. Core point: point containing at least $minPts$ points within eps radius. Border point: neighbor point of a core point with neighbors less than $minPts$ points. Outlier: neither core point nor border point. See [33] for more details.

yields a dense cluster. The aim of this algorithm is to identify the smallest eps grouping of only a single cluster with the chosen $minPts$. The distance between the i -th and j -th optimized designs is defined as follows:

$$a^{ij} = \frac{1}{N_e} \|\gamma^{(i)} - \gamma^{(j)}\|_2 \quad (12)$$

In **Algorithm 1**, a pairwise distance matrix **A** is constructed after calculating the pairwise distances. Subsequently, each row of matrix **A** is sorted in an ascending order, and the smallest value of the $minPts$ -th column is selected as eps . the existence of more than one minimum value in the $minPts$ -th column yields multiple clusters. Thus, in this case, the above procedures are repeated while increasing $minPts$ by one until a single cluster is obtained.

Algorithm 1. Algorithm for selection of parameters in DBSCAN to obtain only a single cluster with the highest density.

Input: $minPts$: Minimum number of designs for a cluster
 $\Gamma = \{\gamma^{(1)}, \gamma^{(2)}, \dots, \gamma^{(n)}\}$: Optimized design dataset

1. Compute a pairwise distance matrix:
 $\mathbf{A} \leftarrow [a^{ij}]_{n \times n}$ where $i = 1, 2, \dots, n$ and $j = 1, 2, \dots, n$
2. Sort each row of **A** in an ascending order:
 $\tilde{\mathbf{A}} \leftarrow [\tilde{a}^{ij}]_{n \times n}$
3. Set the minimum value in the $minPts$ -th column to eps :
 $eps \leftarrow \min(\tilde{a}^{i, minPts})$
 $N \leftarrow$ Number of $minPts$ -th column components with the same values as eps

if $N > 1$ **then**
 $minPts \leftarrow minPts + 1$
 Repeat 1 to 3
end if
return $eps, minPts$

After clustering, the average design of the cluster is determined, as presented in **Fig. 3**. To determine the convergence of the loop of the STO, the integration of errors between the FRFs of the damaged structure and average design over the entire measurement frequency range, $TotalFRFError$, is defined as follows:

$$TotalFRF \text{ error} = \sum_{j=1}^{N_f} \sum_{k=1}^{N_m} \left(\frac{|X_k^*(\omega_j)| - |X_k^{avg}(\omega_j)|}{|X_k^*(\omega_j)|} \right)^2 \quad (13)$$

where $X_k^{avg}(\omega_j)$ and N_f denote the response of the average design at the k -th measurement point and the number of frequency points for all measured FRFs, respectively. This value is typically calculated when the average design is obtained in the STO loop to achieve a convergence of results. When the convergence criterion is satisfied, the loop ends, and the average design is obtained as the damage identification result.

2.3. Damage identification procedure

The damage identification procedure of the STO is illustrated in **Fig. 4**. In the first step, the FRFs of a damaged structure are measured or calculated. Following this, using TO with a set of randomly selected frequency points $\omega^{(n)}$, the n -th optimized design, $\gamma^{(n)}$, is obtained and stored in a database. Note that, random sampling is performed once or repeated several times to obtain diverse local optima during each TO process. Further, several optimized designs are obtained by repeating the above steps. If n is equal to or greater than the set $minPts$, cluster analysis (DBSCAN) is performed. The average design of the cluster is obtained, and the above steps are repeated until $TotalFRFError$ converges.

3. Numerical examples

3.1. Example 1: Beam with a single damaged element

Several optimization problems aimed at identifying structural damage are presented in this section to demonstrate the validity and properties of the presented STO method. These examples also reveal the advantages of the presented STO scheme over the CTO scheme. Equivalent steel material properties are employed: Young's modulus E_0 of 200 GPa, mass density ρ_0 of 7850 kg/m³, and Poisson's ratio of 0.3. The coefficients of Rayleigh damping, α and β , are set as 10^{-2} and 10^{-4} , respectively. Using the STO method, 8–64 frequency points are randomly selected for diverse solutions in the frequency range of 0–400 Hz with the `rand` function in MATLAB. As will be mentioned later in subSection 3.4, the STO scheme is an effective method to increase the accuracy of damage identification by adding more information. Thus, selecting the widest frequency can improve the accuracy of damage identification. However, without the loss of generality, a fixed frequency domain (0–400 Hz) is utilized for following examples; the frequency domain should be changed considering the properties of the problem of interest. To solve each TO problem in the STO and CTO schemes, the method of moving asymptotes is employed [45]. To quantify the accuracy of the damage identification result, $Accuracy$ is defined as follows (see the details of the equation in **A**):

$$Accuracy = \frac{1}{N_d} \sum_{d \in \mathbf{D}} \min \left(1 - \gamma_d^* + \gamma_d, \frac{1 - \gamma_d}{1 - \gamma_d^*} \right) \cdot \left(\frac{1}{N_h} \sum_{h \in \mathbf{H}} \gamma_h \right) \cdot 100(\%) \quad (14)$$

where **D** and **H** denote the sets of indices of damaged and healthy elements in the damaged model, respectively. The numbers of

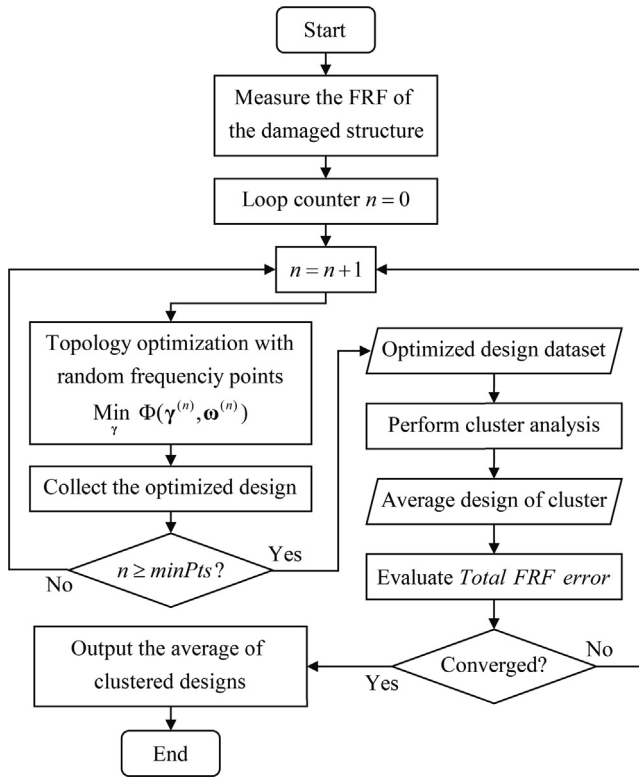


Fig. 4. Procedure of the STO scheme.

damaged elements and healthy elements in the target damaged model are denoted as N_d and N_h , respectively. The design variables of the damaged and damage-identified models are denoted as γ^* and γ , respectively, and the indices of the damaged and healthy elements are denoted by subscripts d and h , respectively. However, in practical applications where the correct answer (location and severity of damage) is unknown or unclear, this *Accuracy* should be carefully used. In order to evaluate the result of damage identification, some of the obtained FRFs (e.g., specific frequency range) can be used in the STO scheme for finding damage, and the accuracy of the result can be assessed by comparing the remaining FRFs with those of the damage identification result.

In the first example, the damage identification problem of a cantilever consisting of one-dimensional beam elements is considered, as illustrated in Fig. 5(a). The design domain is discretized into 15 beam elements. Without loss of generality, a damage state is represented by setting the design variable of the 4th element as 0.5. A unit impulse force is vertically applied to the 2nd node, and the vertical response is recorded at the 13th node to obtain the displacement FRFs. To illustrate the local optima problem, four frequency domains are selected for the CTO scheme. As depicted in Fig. 5(b), several local optima are obtained using the CTO scheme. Note that the *Accuracy* in Eq. (14) of the results varies from 1.0674% to 60.3248% depending on the frequency range selection. Subsequently, as illustrated in Fig. 6, the TO process with a set of randomly sampled frequencies is repeated to obtain the local optima for the STO scheme, and the clustering algorithm with $\text{minPts} = 8$ is applied. Fig. 6(a) illustrates eight clustered designs out of the 32 optimized designs obtained using the STO scheme. Note that the axes presented in Figs. 6(a) and (b) represent the number of elements and the design variables of each element, respectively.

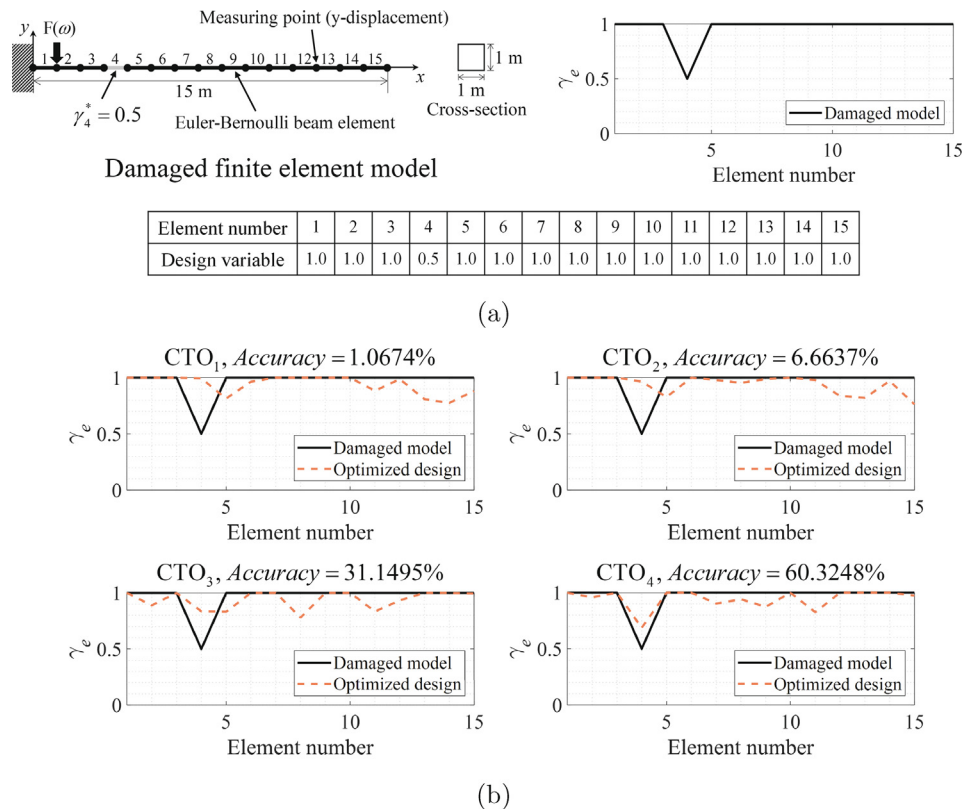


Fig. 5. Beam damage identification problem. (a) Problem definition, (b) comparison of results obtained using CTO with different frequency ranges (CTO₁: 0–100 Hz, CTO₂: 0–400 Hz, CTO₃: 50–200 Hz, and CTO₄: 50–400 Hz with the same interval of 0.5 Hz); refer to B for a detailed discussions. of the results.

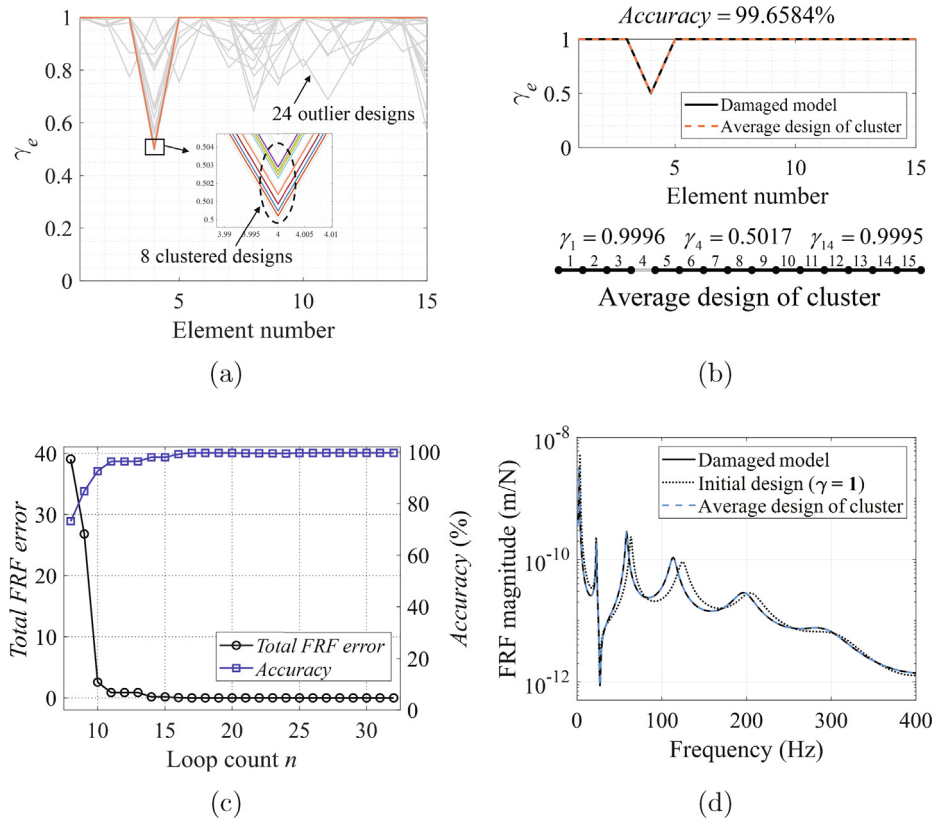


Fig. 6. Damage identification with the STO scheme. (a) Local optima and clustered designs (x-axis: element number and y-axis: design variable value), (b) average design of the cluster, (c) optimization history, and (d) FRFs of the damaged model, initial design, and average design of the cluster.

As presented in Fig. 6(a), eight clustered designs are depicted with different colors (except for gray) for each design, and 24 outlier designs are plotted with gray color. In the present example, eight similar designs are used to construct the single cluster. Fig. 6(b) presents the final average layout of the cluster with an Accuracy of 99.6584%. Figs. 6(c) and (d) present the optimization history and FRFs obtained before and after the optimization with the STO scheme, respectively. The figures reveal successful realization of damage identification.

The selection of the initial *minPts* in the DBSCAN algorithm is important for the damage-identification performance of the STO scheme. Its value should be selected by considering the characteristics of the problem of interest. In the present study, we assume that several local optima close to the global optimum can be obtained using TO. The parameter *minPts* denotes the minimum number of similar local optima distributed around the global optimum. Table 1 summarizes the damage identification results based on the choice of *minPts*. The first example, as illustrated in Fig. 5(a), is solved with different *minPts*, and the results are compared. All the results reveal a high Accuracy. By increasing the value of *minPts*,

the Accuracy tends to decrease, and the number of loop repeat counts increases. Although we cannot determine the optimal *minPts* from this particular result, we set the initial *minPts* as eight in the following examples for the realization of a high identification accuracy and suitable computation time, and the corresponding results are presented in the following examples.

Measuring and excitation node selection

To test the robustness of the developed STO scheme with respect to the selection of measuring and excitation nodes, Fig. 7 (a) illustrates the Accuracy with the changes in the beam. Based on the results, we can conclude that the STO scheme can improve the Accuracy significantly compared to the CTO scheme. However, certain particular cases with low-accuracy values are presented in the table in Fig. 7(a). Although the Accuracy should theoretically be symmetric owing to the symmetry of the FRF matrix, the random number selection in the STO scheme causes an asymmetric distribution of the Accuracy. In addition, interestingly, setting the measuring and excitation points close to the nodal points of the eigenmodes of the beam system further deteriorates the accuracy. For example, the Accuracy of 3.7509% (exciting at the 13th node and measuring at the 15th node) indicated in Fig. 7(a) can be attributed to the nodal points of the 2nd, 5th, and 6th modes, as illustrated in Fig. 7(b). This argument is also related to the maximization of the information on modal parameters to locate the damage (see [37,38] and references therein). In Fig. 8(a), the clustering result shows that the STO fails to identify a set of local optima around the true solution when measuring at the 13th node and exciting at the 15th node. Out of the 19 designs obtained, only three local optima were found close to the global solution, while a cluster of other similar local optimal solutions formed first, creating a cluster far from the actual solution. To address this issue,

Table 1
Damage identification results obtained using the STO scheme based on *minPts*.

<i>minPts</i>	Accuracy (%)	<i>eps</i>	Loop repeat count
2	99.9268	4.4171×10^{-8}	11
4	99.6910	4.2839×10^{-7}	13
8	99.6584	2.8585×10^{-7}	32
16	99.5688	1.9957×10^{-6}	39
32	99.4546	5.8873×10^{-6}	73
64	99.5203	1.0517×10^{-5}	122

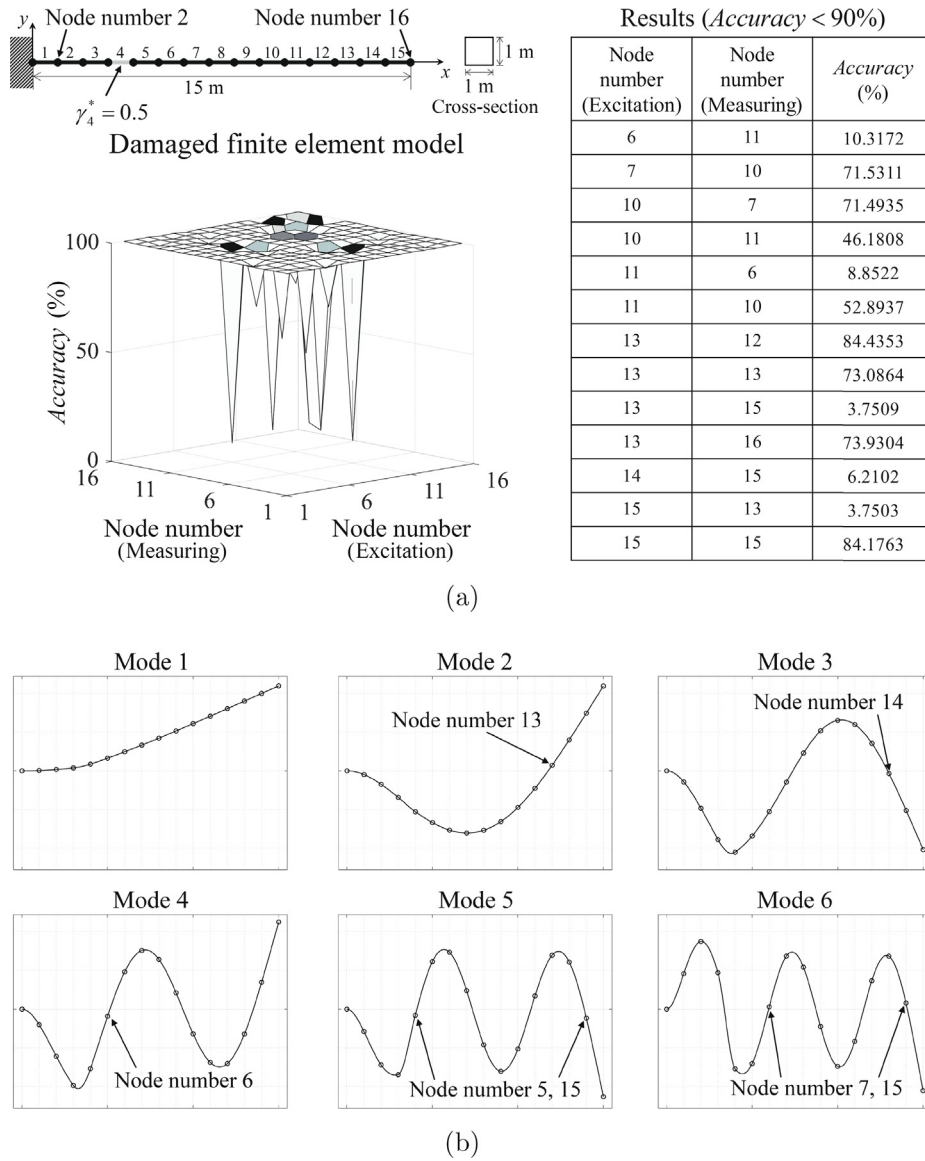


Fig. 7. Test for measuring and excitation node selection. (a) Damaged model and damage identification results according to measuring and excitation nodes and (b) first six mode shapes of the damaged model and their nodal points.

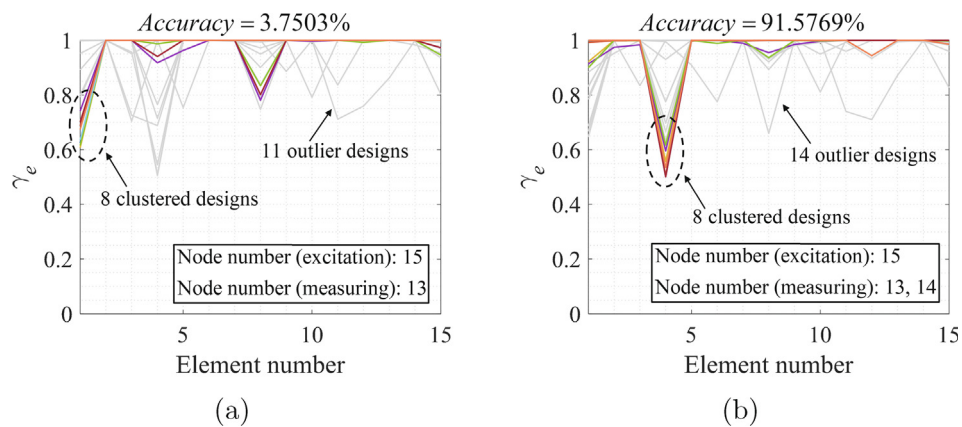


Fig. 8. Comparison of clustering results according to chosen excitation and measuring nodes. (a) Single input and single output and (b) single input and multiple outputs.

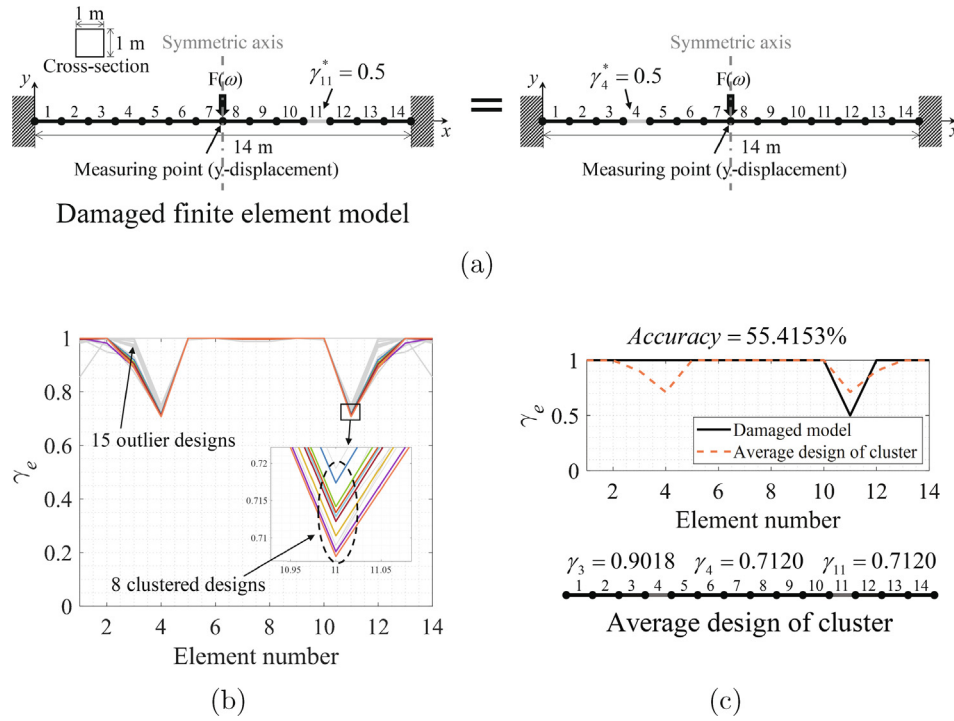


Fig. 9. Damage identification of a beam with symmetric responses. (a) Problem definition, (b) local optima and clustered designs, and (c) average design of the cluster.

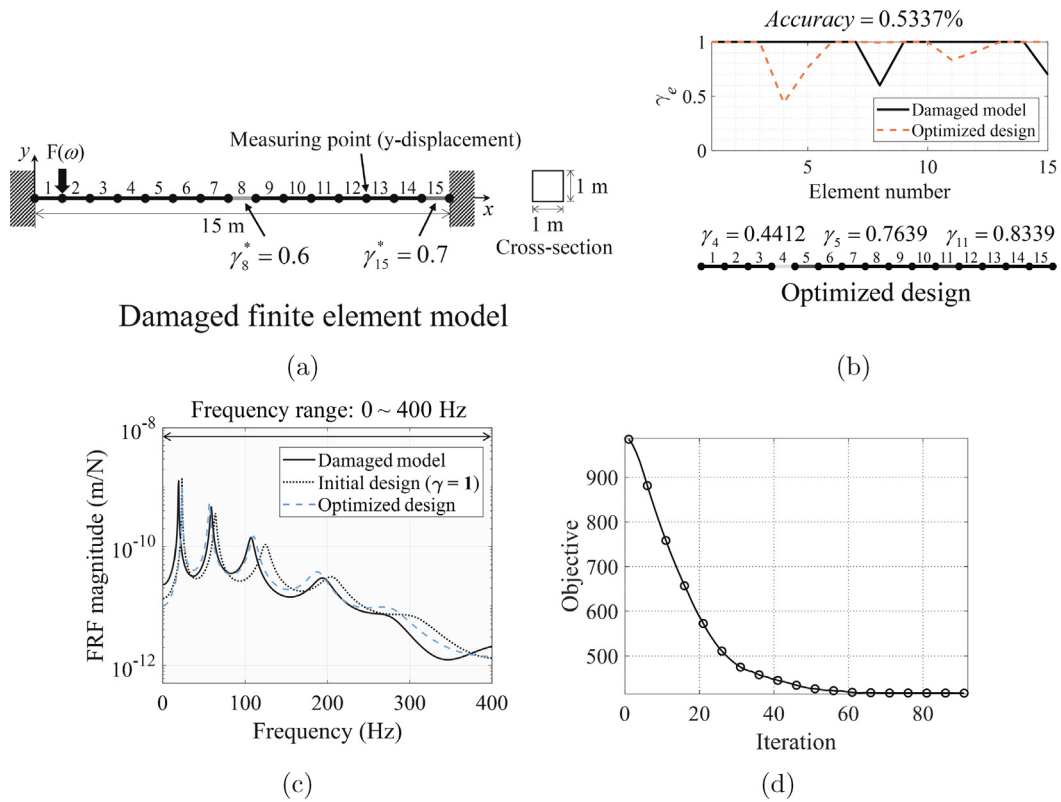


Fig. 10. Damage identification example 2. (a) Problem definition with two damaged elements, (b) optimized design obtained from the CTO procedure, (c) FRFs of the damaged model, initial design, and optimized design, and (d) optimization history.

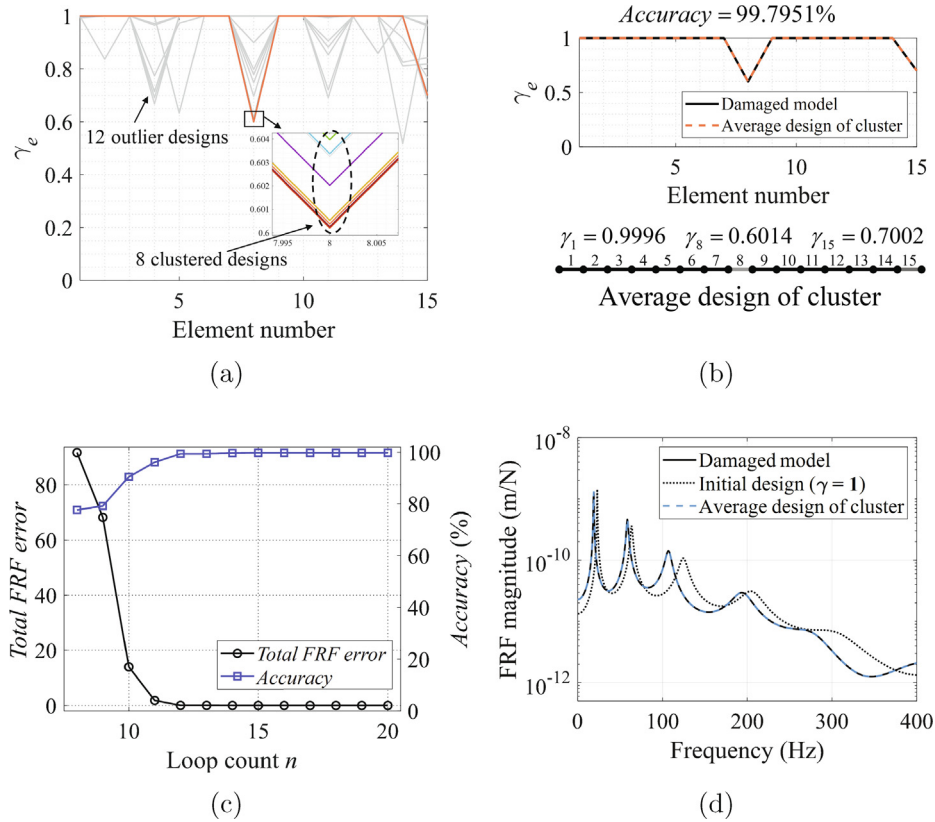


Fig. 11. Damage identification with the STO. (a) Local optima and clustered designs, (b) average design of the cluster, (c) optimization history, and (d) FRFs of the damaged model, initial design, and average design of the cluster.

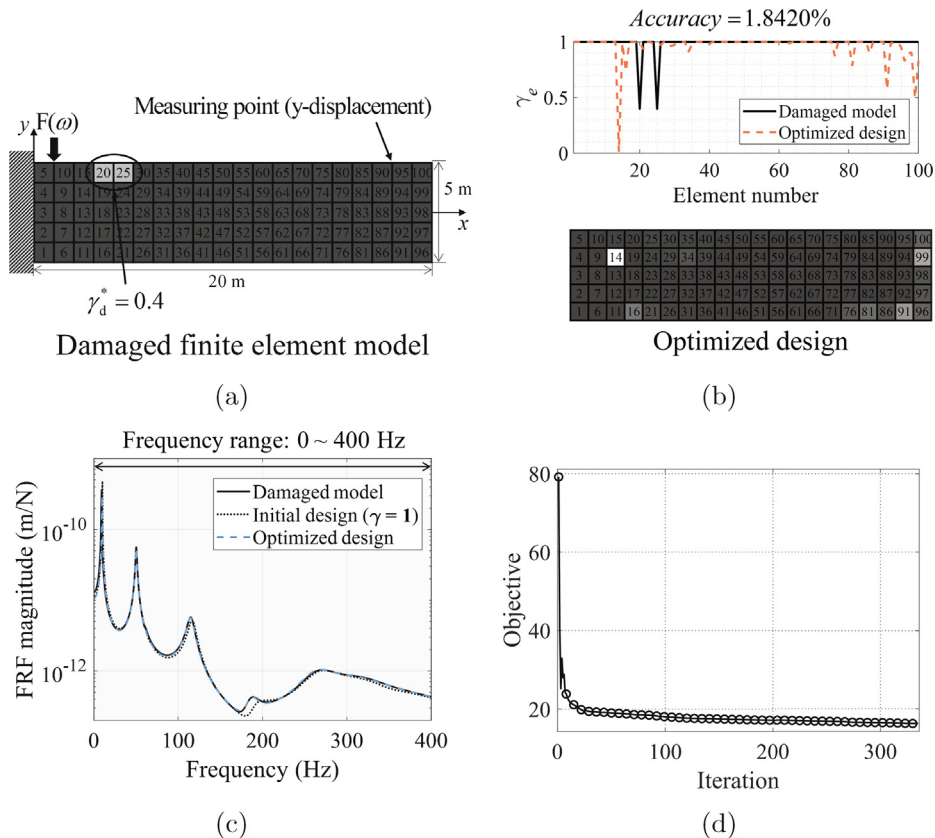


Fig. 12. Damage identification results in a two-dimensional domain. (a) Damaged model, (b) optimized design obtained from the CTO procedure, (c) FRFs of the damaged model, initial design, and optimized design, and (d) optimization history.

an additional measuring node was selected, as demonstrated in Fig. 8(b). By adding more information (specifically, a measuring point at the 14th node), local optima similar to the true solution were collected, resulting in an accuracy of 91.5769%. Furthermore, the *eps* values of Fig. 8(a) and (b) are 0.0024 and 0.0007, respectively, indicating that the cluster around the global optimum is denser than other clusters. To improve the accuracy of the proposed method, it is important to select the appropriate number and positions of measurement and excitation points, in addition to adding more information. The sum of the sensitivity of FRFs in selected frequency ranges can be an objective function to maximize the information of structural damage [46], and it can easily be combined with the proposed method. However, the target frequencies are randomly selected in each optimization process of the STO scheme, and further research is necessary to improve this process, such as by utilizing both the sum of sensitivity and its variance in the frequency domain.

Test on a symmetric system

The effect of system symmetry on the STO scheme is illustrated in Fig. 9. An asymmetric damage state excluding the center measuring and excitation nodes is considered. Specifically, all conditions (boundary and measuring conditions) except the location of damage are symmetric. Therefore, the responses of the systems with right (the 11th element) and left (the 4th element) damage states are identical. With the STO scheme, the damage caused to the right and left elements are found with an *Accuracy* of 55.4153%. This can be attributed to the symmetry of the sensitivity values with even initial design variables ($\gamma = 1$). Therefore, in the STO scheme, it is often effective to select asymmetric boundary conditions, geometrically uneven initial variables, and multiple

inputs and outputs. However, to the best of our knowledge, in practice, for damage identification, multiple inputs and outputs are typically employed to deal with a symmetric case.

3.2. Example 2: beam with multi-damaged elements

As the next example, a case of multiple damage states is considered. In this example, two damaged elements are assumed, as illustrated in Fig. 10(a). Without loss of generality, the design variables of the 8th and 15th elements are set as 0.6 and 0.7, respectively. Fig. 10 illustrates the damage identification results obtained using the CTO scheme. Owing to the local optima issue, a local optimum with an Accuracy of 0.5337% far from the target damaged model is obtained, as depicted in Fig. 10(b). The FRFs of the optimized design are also located far from the target FRFs, as presented in Fig. 10(c), and the optimization history of the CTO scheme is illustrated in Fig. 10(d). The developed STO scheme is illustrated in Fig. 11. Owing to the local optima issue, 12 designs located far from the target damaged model can be obtained, as shown in Fig. 11(a). The clustering algorithm classifies these designs as outliers. However, the STO scheme determines eight designs that are close to the damaged model, as presented in Fig. 11(a). The Accuracy of the average design is 99.7951%. The average FRFs of the clustered designs also match well with those of the damaged model.

3.3. Example 3: two-dimensional beam with minimal damage

In this example, the damage identification problem in a two-dimensional domain with little damage is considered, as illustrated in Fig. 12(a). The target damaged model consists of 100 linear plane

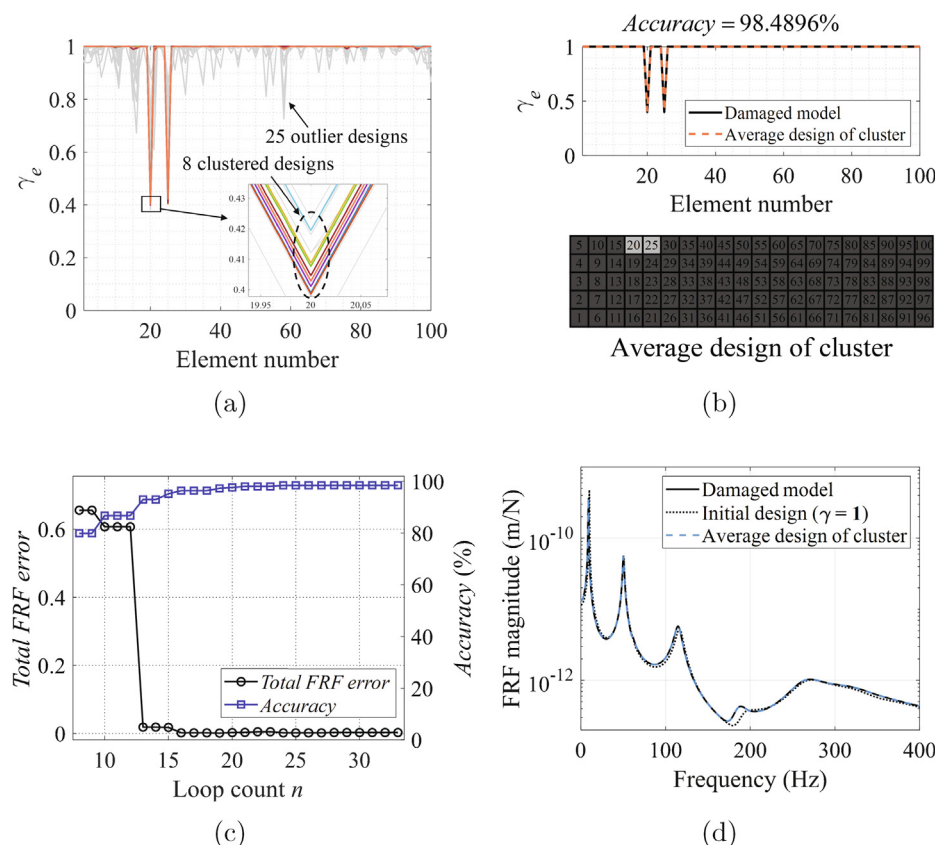


Fig. 13. STO scheme. (a) Results of clustering analysis, (b) average design of cluster, (c) optimization history, and (d) FRFs of the damaged model, initial design, and average design of the cluster.

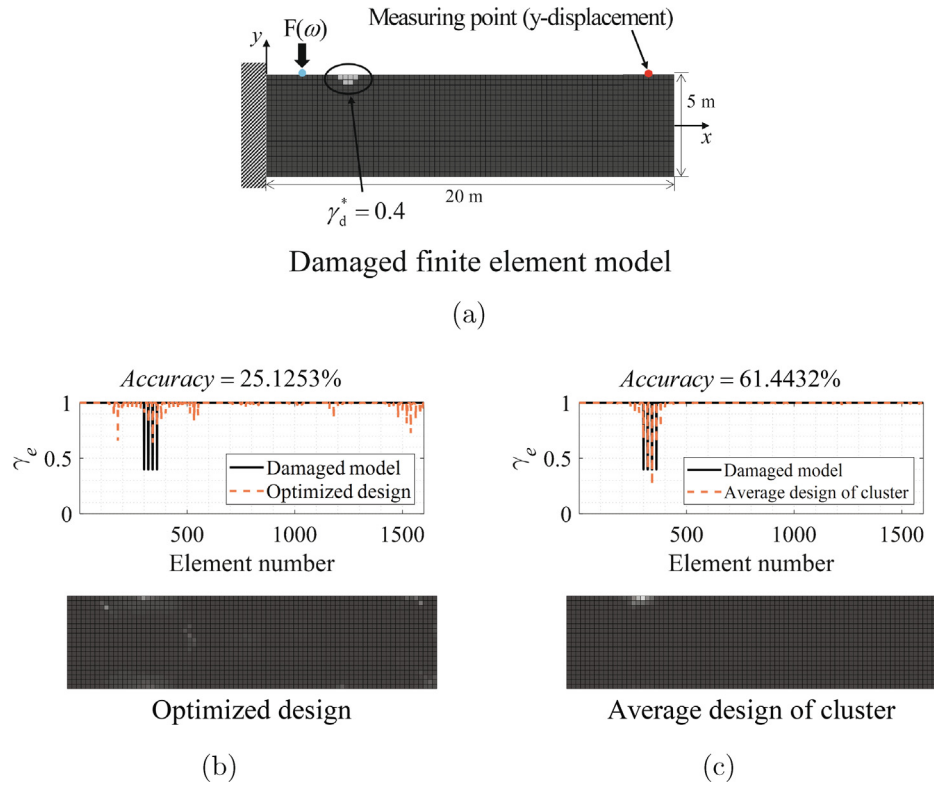


Fig. 14. Damage identification results of the mesh refined FE model. (a) Damaged FE model, (b) optimized design from the CTO scheme, and (c) average design of the cluster from the STO scheme.

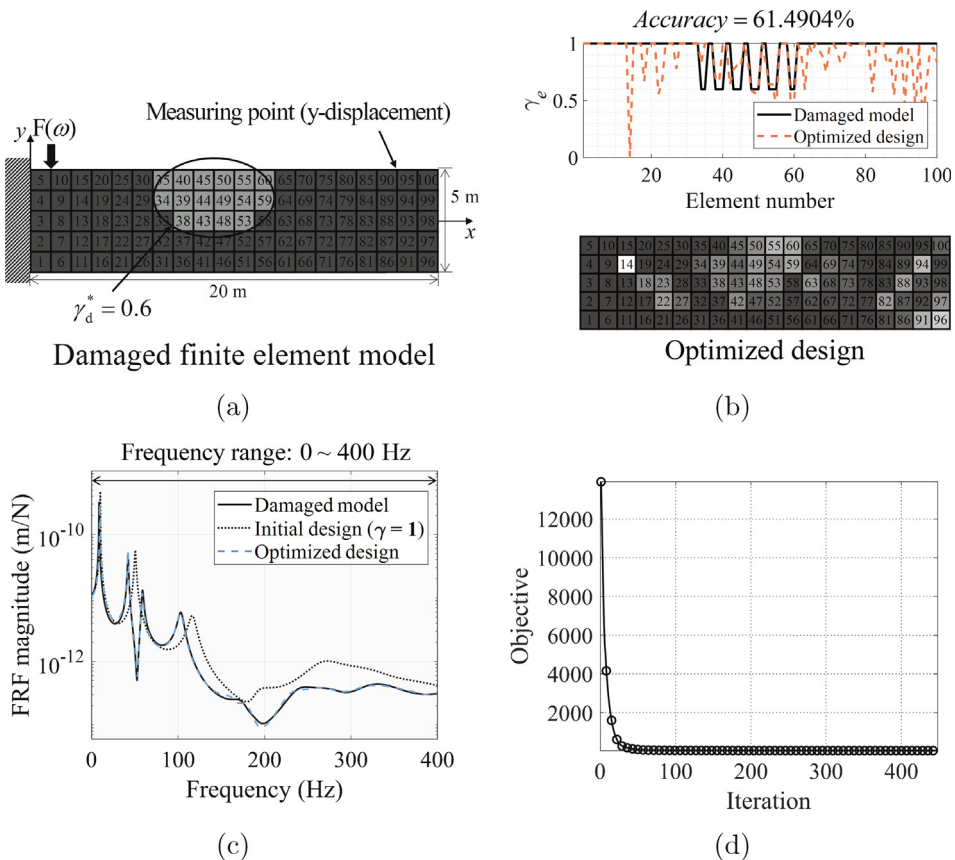


Fig. 15. Example 4 with significant damage. (a) Problem definition, (b) optimized design, (c) FRFs of the damaged model, initial design, and optimized design, and (d) optimization history.

stress elements, and the design variables of the 20th and 25th elements are set as 0.4 each, representing minimal damage. A density value of 0.4 is chosen arbitrarily; however, the findings of the CTO and STO schemes presented herein can be applied to other types of damage with varying density values. The objective of this optimization problem is the same as that of a one-dimensional problem, i.e., damage identification using TO. Fig. 12(b) and (c) illustrate the optimized layout in a frequency domain ranging from 0 to 400 Hz. Note that the responses of the optimized design are sufficiently close to those of the damaged model. However, owing to the negligible effect of damage, the differences in the responses of the damaged model, initial design, and optimized design are minimal. Thus, it is difficult for the local optimizer to identify the damaged parts, and the *Accuracy* is low (1.8420%). This example, yet again, reveals the limitation of the CTO scheme with respect to the identification of a local optimized layout with a similar response owing to the local optima problem in TO, slight modifica-

tions in responses by relatively minimal damage, and inadequate comparison of insufficient vibration-related information.

To overcome this difficulty, the STO scheme is applied, as presented in Fig. 13, with $\minPts = 8$ and $\epsilon ps = 4.6078 \times 10^{-6}$. The eight most similar designs are grouped as a cluster, and the other 16 designs are classified as outliers. The local optimized layouts are presented in Fig. 13(a). Because the size of the damage considered in Fig. 12(a) is small compared with the characteristic length, a local optimum having similar responses to that of damaged model but far from the damaged structure can be obtained as shown in Fig. 12(b). However, the clustering algorithm can successfully identify the cluster containing the damaged model, as presented in Fig. 13(b), with an *Accuracy* of 98.4896%. Fig. 13(c) reveals the *TotalFRFError* and *Accuracy* of the STO procedure. Notably, the responses match those of the damage model reasonably well, as illustrated in Fig. 13(d). Note that the responses of these models are extremely similar to those presented in Fig. 12, and it is revealed that the present method is effective to identify slight damage of structures compared with the existing approach.

To further validate the present method in a more realistic scenario, we consider a mesh refined model (80 by 20) with minimal damage. The density of the damaged area is set to 0.4, as depicted in Fig. 14(a). We use the same parameters and material properties as in the previous examples, with blue and red circles marking the excitation and measuring points, respectively. Fig. 14(b) and (c) present the optimization results from the CTO and STO schemes, respectively. It is noteworthy that the STO scheme successfully identifies the damage, achieving an *Accuracy* (Accuracy) of 61.4332%.

3.4. Example 4: two-dimensional beam with significant damage

In the fourth example, a two-dimensional beam with significant damage is considered by setting the density of the gray elements as 0.6, as shown in Fig. 15(a). The problem definition and the boundary condition are set as the same as those in the previous example. Using the CTO scheme with a frequency range from 0 Hz to 400 Hz, the optimized layout and its responses are obtained, which are shown in Figs. 15(b) and (c), respectively as illustrated, the *Accuracy* of 61.4904% is achieved.

The STO scheme with $\minPts = 8$ and $\epsilon ps = 0.0154$ is used, as shown in Fig. 16. Fig. 16(b) shows the average layout. Although several gray elements are observed, the damage is successfully identified. The *Accuracy* is approximately 66.0725%. The relatively

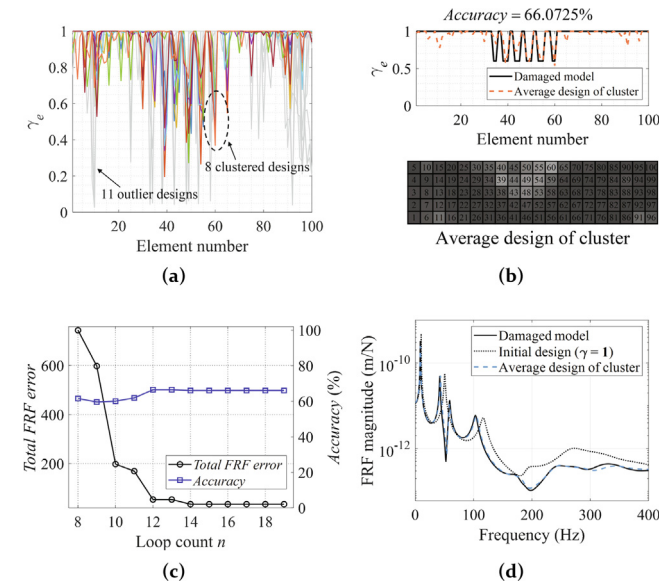


Fig. 16. Example 4 with the STO scheme. (a) Results of cluster analysis, (b) average design of the cluster, (c) optimization history, and (d) FRFs of the damaged model, initial design, and average design of the cluster.

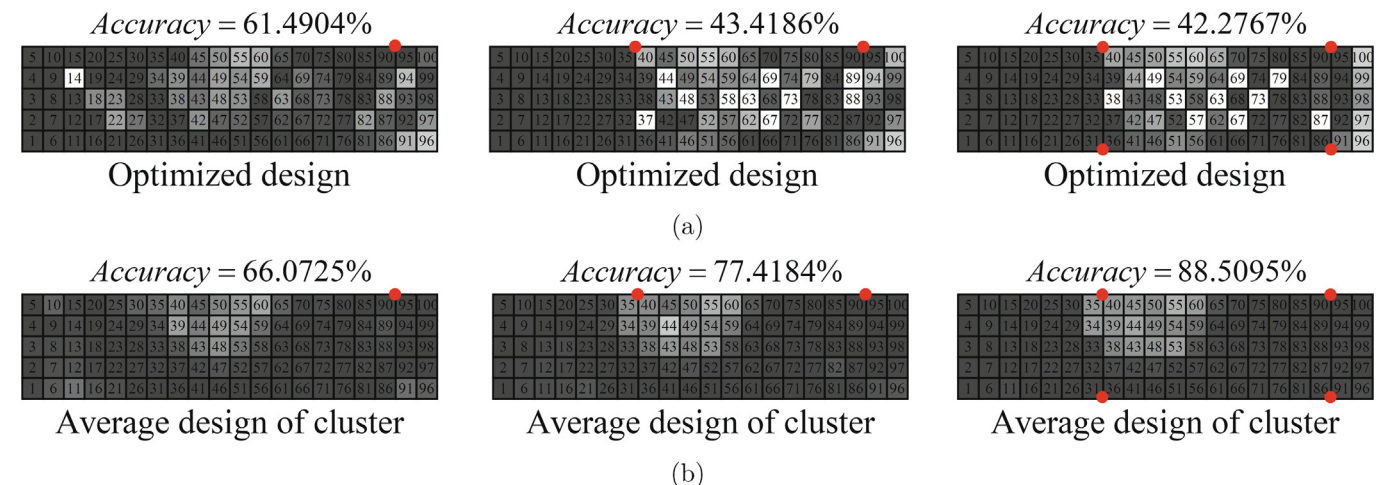


Fig. 17. Comparison of results obtained with multiple measuring points (measuring points: red dots). (a) Optimized designs obtained from the CTO scheme, and (b) averaged designs obtained from the STO scheme.

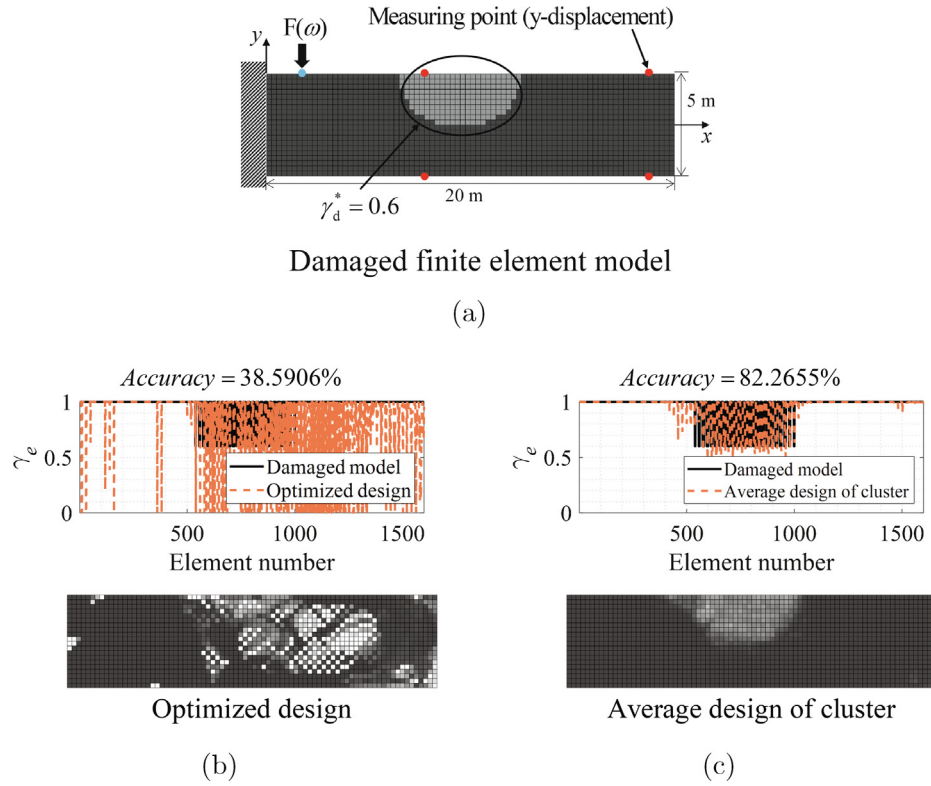


Fig. 18. Damage identification results. (a) Damaged FE model, (b) optimized design with the CTO scheme, and (c) average design of the cluster with the STO scheme.

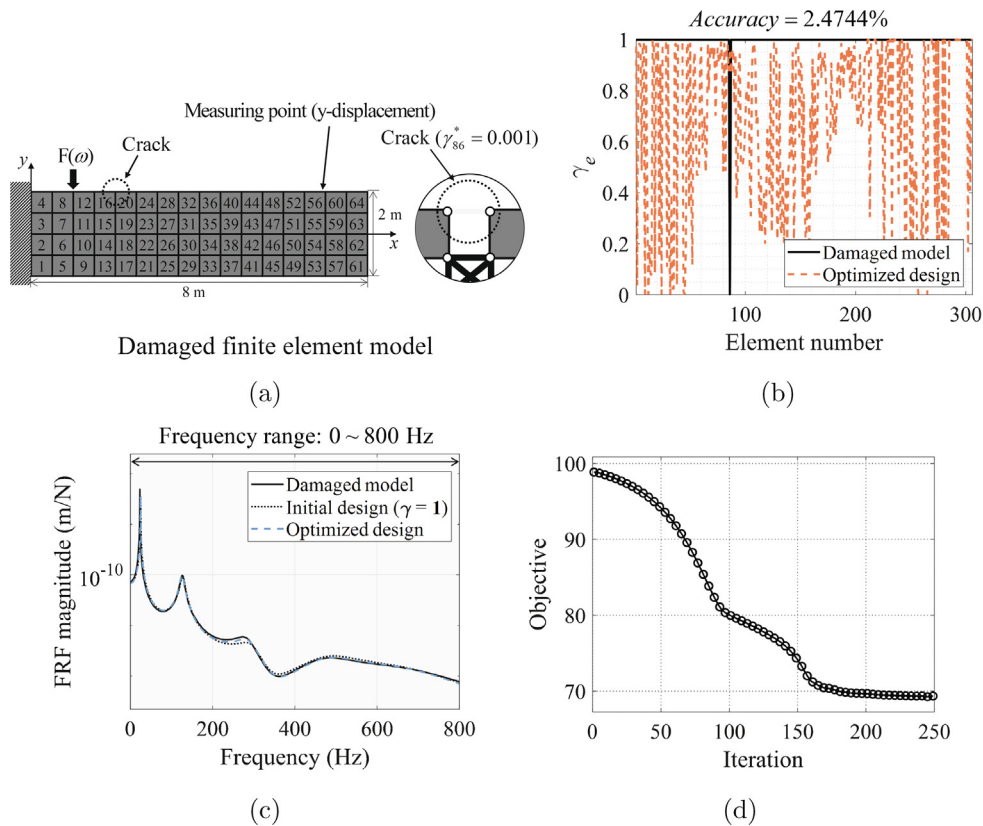


Fig. 19. Damage identification of an open cracked beam. (a) Open damaged model, (b) optimized design with the CTO, (c) FRFs of the damaged model, initial design, and optimized design, and (d) optimization history.

low Accuracy is attributed to the optimization formulation in Eq. 7 assuming a smaller damage by adding $\lambda \sum_{e=1}^{N_e} (1 - \gamma_e)$. However, from a practical perspective, as severe damage cause large differences in structural responses, it is easier to find damage, and relatively high Accuracy is obtained by CTO scheme in Fig. 15. From a theoretical perspective, as significant damaged model is far from the initial intact design, the convergence to a global solution is difficult than the previous examples, and several combinations of intermediate design variables around the damage state can be assumed to exist to reasonably approximate the target FRF curve. A comparison of the FRFs reveals that the curve of the averaged design of the cluster matches well with that of the damaged model, as shown in Fig. 16(d).

To improve the accuracy, additional information should be provided to the optimization formulation strategy. For example, responses should be measured at multiple points, i.e., multiple inputs and outputs must be recorded. To illustrate this concept, Figs. 17(a) and (b) present the optimized results obtained by increasing the number of outputs, which are marked as red dots in Fig. 17, to one, two, and four. Fig. 17(a) presents the optimization results obtained using the CTO scheme; noticeably, the layouts are adversely deteriorated with increasing number of measuring points. In the STO scheme, increasing the number of measuring points improves the Accuracy of the prediction, which illustrates the nature of the damage identification problem and the STO scheme. This is in line with the known fact that in the engineering field, increasing the number of input and output points is known to increase the accuracy and probability of damage identification.

In Fig. 18, the mesh refined FE model (80 by 20) with a large damage is considered. As shown in Fig. 18(a), one excitation node and four measuring points are selected with the same problem definition of the previous examples. Frequency points are randomly selected for every 20 iterations during each sub-TO problem, and the optimization results with the CTO and STO schemes are presented in Fig. 18(b) and (c). The higher Accuracy of 82.2655% is achieved by the STO scheme.

3.5. Example 5: open cracked beam

In the final example, the damage identification problem of a two-dimensional open cracked cantilever is considered as shown in Fig. 19(a). Each finite elements are connected with artificial links, and a crack is modeled by setting the 86th design variable as 0.001. Through the CTO scheme with a frequency range from 0 to 800 Hz, the damage identification result and FRFs before and after optimization are illustrated in Fig. 19(b) and (c), respectively, and the optimization history is presented in Fig. 19(d). While the FRF of the optimized design get closer to the FRF of damaged model, the poor Accuracy of 2.4744% is obtained due to the local optima issue. Then, the STO scheme is applied in Fig. 20 with $minPts = 8$ and $eps = 0.027$. In this example, random sampling of frequency points is repeated for every 20 iterations during each TO. Although there are several intermediate design variables, the damage is identified with the Accuracy of 92.1565% which is much higher than that of the CTO method. The optimization history and FRFs of the results are depicted in Fig. 20(c) and (d).

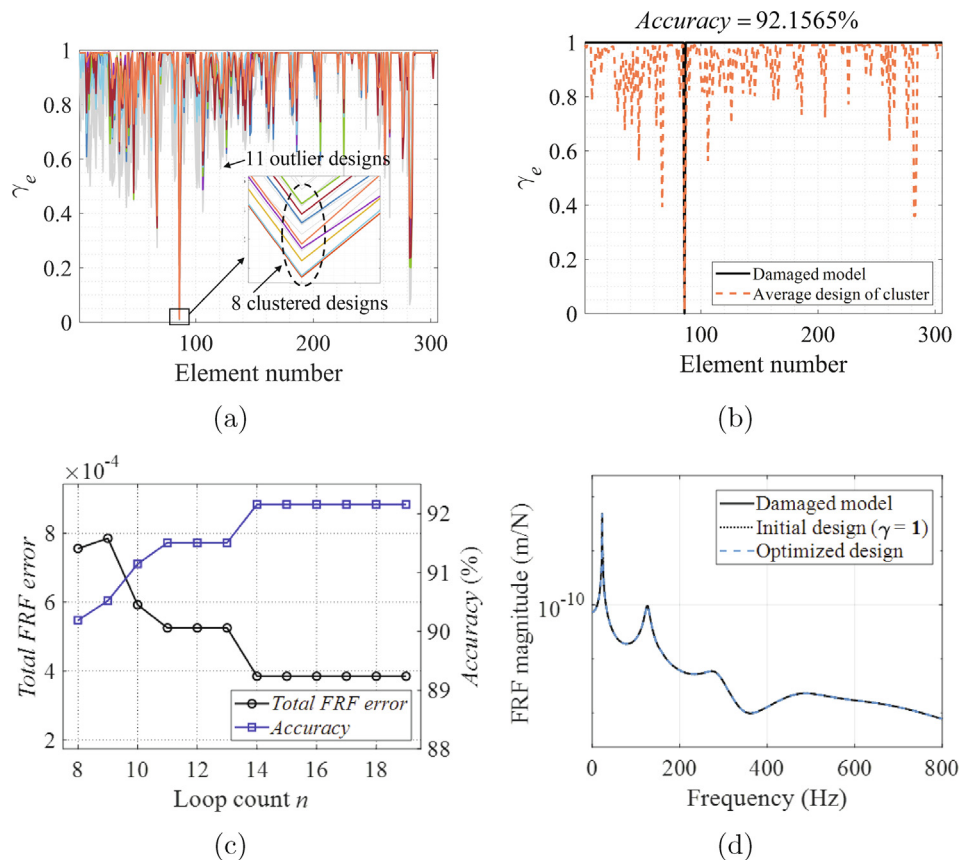


Fig. 20. Damage identification with the STO scheme. (a) Result of clustering, (b) average design of the cluster, (c) optimization history, and (d) FRFs of the damaged model, initial design, and average design of the cluster.

4. Conclusion

Combining the STO scheme and the clustering algorithm, this research presents a new STO scheme that statistically collects and analyzes locally optimized layouts is developed for structural damage identification. In the CTO scheme adopted for damage identification, we generally experience difficulties owing to the local optima problem in TO, slight modifications in responses caused by relatively minimal damage, and inadequate comparison of insufficient vibration-related information. Therefore, identifying damage or solving the inverse problem of identifying damage using the current TO scheme is often complicated. In the present study, to address these difficulties, an STO scheme is developed by combining the STO scheme and the clustering algorithm. It is known that a global optimum (a target damaged structure) of an optimization formulation exists uniquely regardless of the chosen frequency domain. Therefore, numerous local optima from a series of TO problems with different frequencies of interest are obtained, and from a statistical perspective, we assume that similar local optima appear near the global optimum; however, this argument may not always be true. Nonetheless, based on several optimization examples, it is demonstrated that the developed approach improves the prediction accuracy of damage identification, which is one of the primary contributions of this study. In detail, the present study reveals the following:

- The developed statistical approach improves the damage prediction accuracy. Similar optimized designs are grouped as a cluster using the DBSCAN algorithm (a clustering algorithm), and the average design of the cluster is presented as the damage identification result.
- The frequency domain of the optimization problems is a key factor affecting the *quality* of the local optimum, i.e., the closeness of the local optimum to the global optimum (or the true solution with damage).
- A selection of multiple inputs and outputs improves the accuracy of the local optimum. Thus, for damage identification, a strategy involving variations in the measuring and impact points can be effective. However, selecting nodal points of eigenmodes of structures as the measuring points can deteriorate the prediction accuracy.
- Large-scale damage can significantly affect the FRF curves, whereas small-scale damage only slightly modifies them. With the present approach, successful identification of small-scale damage can be realized.
- The two types of structural damage, i.e., material damage and an open crack, are successfully identified by the present scheme.

In summary, herein, by solving one- and two-dimensional problems, the developed STO scheme is validated. In future research, this approach can be employed for multiscale TO. From a practical perspective, the integration of the present STO scheme with experimental data should also be studied.

Data availability

The authors are unable or have chosen not to specify which data has been used.

Declaration of Competing Interest

The authors declare that they have no known competing financial interests or personal relationships that could have appeared to influence the work reported in this paper.

Acknowledgments

This work was supported by the National Research Foundation of Korea (NRF) grant funded by the Korea government (MSIT) (NRF-2019R1A2C2084974) and (No.2018R1A5A7025522).

Appendix A. Accuracy evaluation

In the present study, *Accuracy*, as defined in Eq. (14), is used to evaluate the accuracy of damage identification results. Fig. 21 illustrates the accuracy evaluation procedure. The damaged model and the model used to evaluate the accuracy (the result of damage identification) are illustrated in Fig. 21(a). The accuracy of each element is determined, as shown in Fig. 21(b), considering both the location and extent of the damage. If the design variable of the damaged element (element 3 in this example) is predicted to be one, the accuracy is calculated to be zero; if the value is predicted to be zero, this implies that the location of damage is identified even if the value is wrong; therefore, it is calculated as $1 - \gamma_e^*$. As presented in the first equation in Fig. 21(c), averaging the accuracy of each element results in high accuracy (62.5%), even though no actual damage is identified. Thus, in this study, the *Accuracy* is defined as the product of the accuracy of the elements with and without damage (damaged and healthy elements), as presented in the second equation in Fig. 21(c).

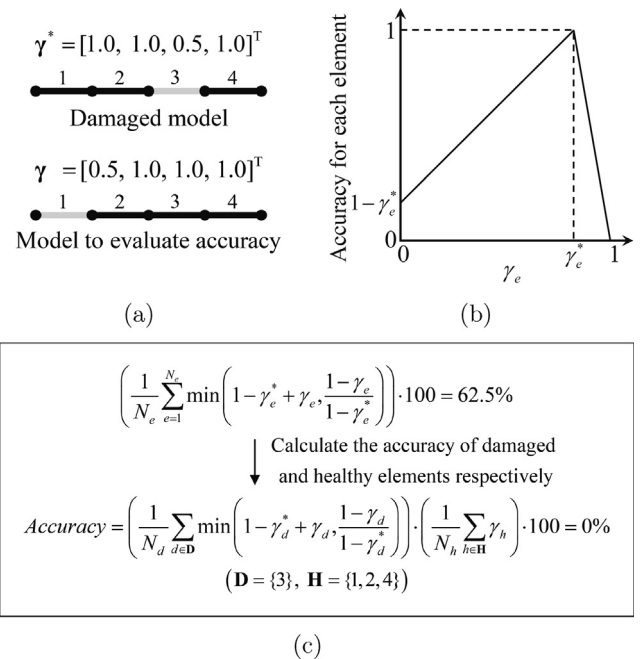


Fig. 21. Example of the accuracy calculation. (a) Damaged model and model employed to evaluate the accuracy, (b) accuracy of each element, and (c) calculation of Accuracy.

Appendix B. Local optima issue

This section describes the local optimum problem that occurs in TO during damage identification. In the optimization problem of damage identification using FRFs, it is important to set the frequency domain of interest. To demonstrate the problems encountered by the conventional method, four frequency ranges (1st range: 0–100 Hz, 2nd range: 0–400 Hz, 3rd range: 50–200 Hz, and 4th range: 50–400 Hz) with the same sampling interval (0.5 Hz) are selected and tested in the problem, as presented in Fig. 5 (a). In Fig. 22, the FRFs of the damaged model, initial intact design ($\gamma = 1$), and optimized design are indicated as solid, dotted, and dashed lines, respectively, and the selected frequency ranges are marked in gray. The optimization problems for the chosen frequency domains are solved, and the optimized layouts are presented in Fig. 23. The results are depicted in Figs. 22 and 23, and the difference between the optimized designs obtained, even when similar frequency ranges are selected, is significant, as illustrated in Figs. 23(b) and (d). The cause of this discrepancy lies in the frequency range where the FRF changes rapidly around the first natural frequency (2.6616 Hz) during the optimization process. Even a

small change in the FRF around the natural frequency can result in a substantial increase in the objective function [34]. The difference between the optimized designs obtained, even when similar frequency ranges are selected, is significant. The cause of this discrepancy lies in the frequency range where the FRF changes rapidly around the first natural frequency (2.6616 Hz) during the optimization process. The complexity of FRFs makes it challenging to choose an appropriate frequency range for damage identification, and the following can be observed. The results are depicted in Figs. 22 and 23, and the following can be observed.

- Based on the optimization formulation, several local optima far from the damaged model are obtained depending on the chosen frequency domain. Even if an optimized design with a sufficiently small objective function value is obtained, the optimized layout can be a local optimum, and selecting an appropriate frequency domain for damage identification is difficult.
- In principle, a gradient-based optimizer may identify damage by considering the response functions.
- The FRFs of the optimized layouts are the approximated responses of the FRFs of the damaged model.

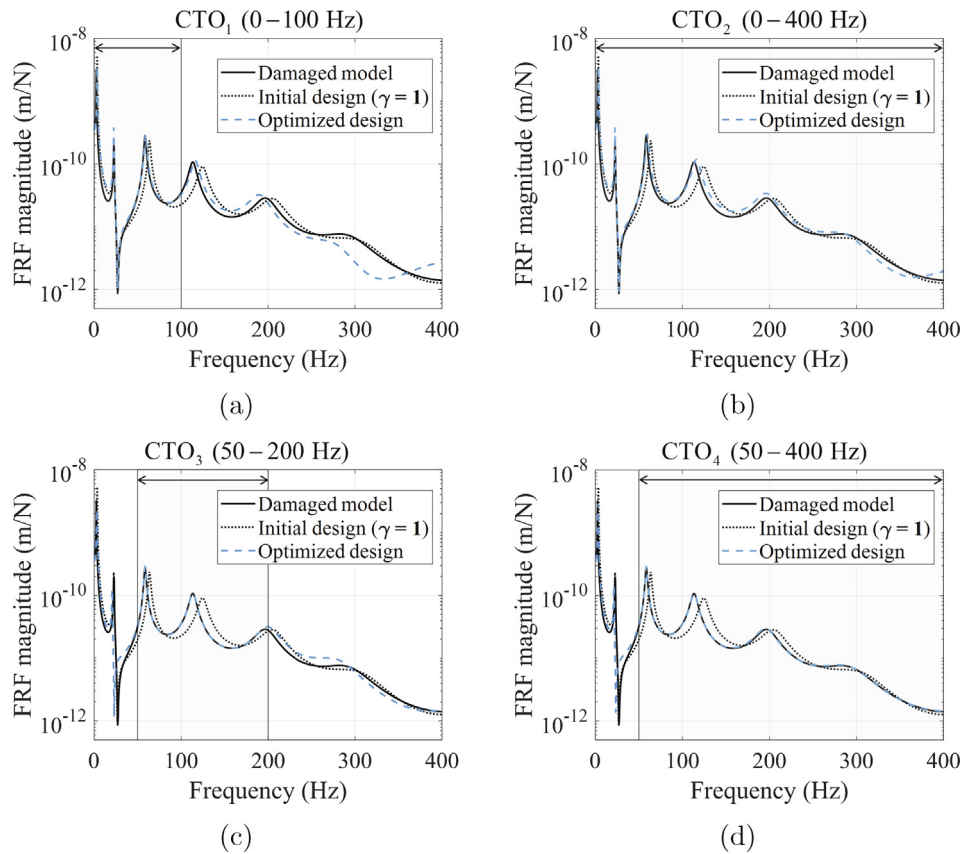


Fig. 22. Local optima problem in the structural TO method depending on the selection of the frequency domain.

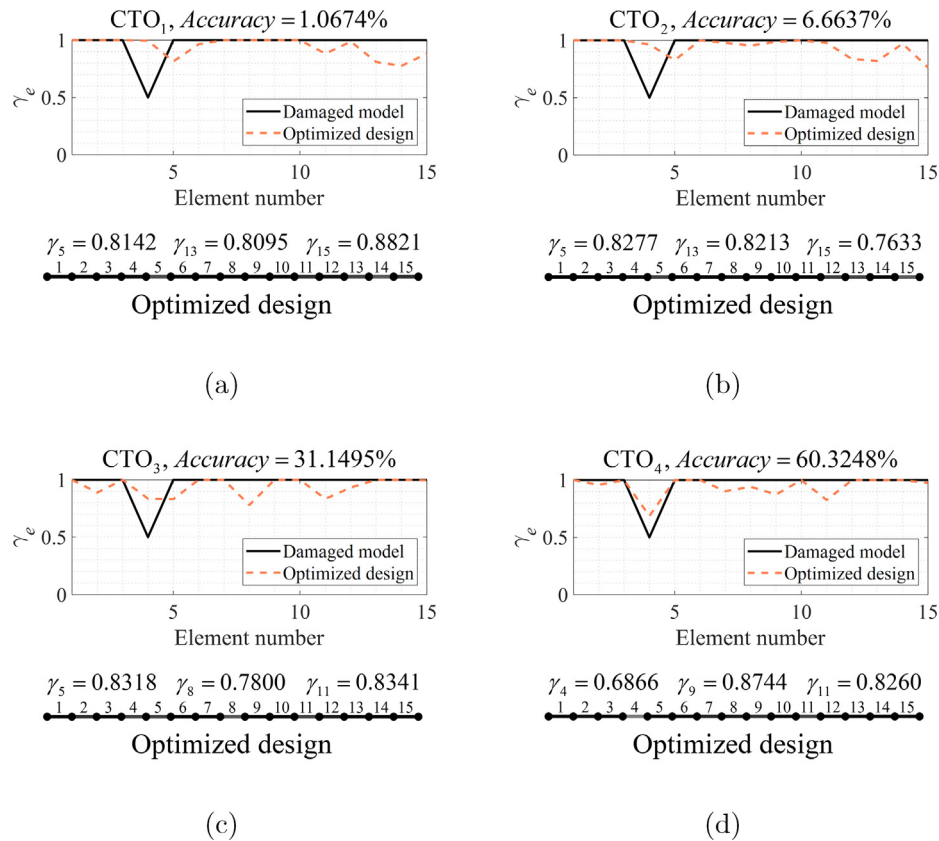


Fig. 23. Optimized designs obtained depending on the selection of frequency range. (a): 0–100 Hz, (b): 0–400 Hz, (c): 50–200 Hz, and (d): 50–400 Hz (with the same interval of 0.5 Hz).

References

- [1] Doebling SW, Farrar CR, Prime MB, Shevitz DW. Damage identification and health monitoring of structural and mechanical systems from changes in their vibration characteristics: a literature review; 1996.
- [2] Doebling SW, Farrar CR, Prime MB. A summary review of vibration-based damage identification methods. *Shock Vib Digest* 1998;30(2):91–105.
- [3] Yan Y, Cheng L, Wu Z, Yam L. Development in vibration-based structural damage detection technique. *Mech Syst Signal Process* 2007;21(5):2198–211.
- [4] Fan W, Qiao P. Vibration-based damage identification methods: a review and comparative study. *Struct Health Monitor* 2011;10(1):83–111.
- [5] Joshuva A, Sugumaran V. A comparative study of bayes classifiers for blade fault diagnosis in wind turbines through vibration signals. *Struct Durab Health Monitor* 2017;11(1):69.
- [6] Lee JS, Kim JE, Kim YY. Damage detection by the topology design formulation using modal parameters. *Int J Numer Methods Eng* 2007;69(7):1480–98.
- [7] Niemann H, Morlier J, Shahdin A, Gourinat Y. Damage localization using experimental modal parameters and topology optimization. *Mech Syst Signal Process* 2010;24(3):636–52.
- [8] Nishizu T, Takezawa A, Kitamura M. Eigenfrequency-based damage identification method for non-destructive testing based on topology optimization. *Eng Optim* 2017;49(3):417–33.
- [9] Ryuzono K, Yashiro S, Nagai H, Toyama N. Topology optimization-based damage identification using visualized ultrasonic wave propagation. *Materials* 2019;13(1):33.
- [10] Ryuzono K, Yashiro S, Onodera S, Toyama N. Performance evaluation of crack identification using density-based topology optimization for experimentally visualized ultrasonic wave propagation. *Mech Mater* 2022;172:104406.
- [11] Dizaji M, Alipour M, Harris D. Subsurface damage detection and structural health monitoring using digital image correlation and topology optimization. *Eng Struct* 2021;230:111712.
- [12] Sampaio R, Maia N, Silva J. Damage detection using the frequency-response-function curvature method. *J Sound Vib* 1999;226(5):1029–42.
- [13] Ratcliffe CP. A frequency and curvature based experimental method for locating damage in structures. *J Vib Acoust* 2000;122(3):324–9.
- [14] Zang C, Imregun M. Combined neural network and reduced frf techniques for slight damage detection using measured response data. *Arch Appl Mech* 2001;71(8):525–36.
- [15] Zang C, Imregun M. Structural damage detection using artificial neural networks and measured frf data reduced via principal component projection. *J Sound Vib* 2001;242(5):813–27.
- [16] Padil KH, Bakhary N, Abdulkareem M, Li J, Hao H. Non-probabilistic method to consider uncertainties in frequency response function for vibration-based damage detection using artificial neural network. *J Sound Vib* 2020;467:115069.
- [17] Zhao B, Cheng C, Peng Z, Dong X, Meng G. Detecting the early damages in structures with nonlinear output frequency response functions and the cnn-lstm model. *IEEE Trans Instrum Meas* 2020;69(12):9557–67.
- [18] Kim D-Y, Woo Y-J, Kang K, Yoon GH. Failure diagnosis system using a new nonlinear mapping augmentation approach for deep learning algorithm. *Mech Syst Signal Process* 2022;172:108914.
- [19] Hakim S, Razak HA. Frequency response function-based structural damage identification using artificial neural networks—a review. *Res J Appl Sci, Eng Technol* 2014;7(9):1750–64.
- [20] Das S, Saha P, Patro S. Vibration-based damage detection techniques used for health monitoring of structures: a review. *J Civil Struct Health Monitor* 2016;6(3):477–507.
- [21] Das S, Roy K. A state-of-the-art review on frf-based structural damage detection: Development in last two decades and way forward. *Int J Struct Stab Dyn* 2022;22(02):2230001.
- [22] Fritzen C-P, Jennewein D, Kiefer T. Damage detection based on model updating methods. *Mech Syst Signal Process* 1998;12(1):163–86.
- [23] Sipple JD, Sanayei M. Finite element model updating using frequency response functions and numerical sensitivities. *Struct Control Health Monitor* 2014;21(5):784–802.
- [24] Shadan F, Khoshnoudian F, Esfandiari A. A frequency response-based structural damage identification using model updating method. *Struct Control Health Monitor* 2016;23(2):286–302.
- [25] Wang J, Wang C, Zhao J. Frequency response function-based model updating using kriging model. *Mech Syst Signal Process* 2017;87:218–28.
- [26] Alkayem NF, Cao M, Zhang Y, Bayat M, Su Z. Structural damage detection using finite element model updating with evolutionary algorithms: a survey. *Neural Comput Appl* 2018;30:389–411.
- [27] Raut NP, Kolekar A, Gombi S. Optimization techniques for damage detection of composite structure: a review. *Mater Today: Proc* 2021;45:4830–4.
- [28] Chou J-H, Ghaboussi J. Genetic algorithm in structural damage detection. *Comput Struct* 2001;79(14):1335–53.
- [29] He R-S, Hwang S-F. Damage detection by an adaptive real-parameter simulated annealing genetic algorithm. *Comput Struct* 2006;84(31–32):2231–43.
- [30] Wei Z, Liu J, Lu Z. Structural damage detection using improved particle swarm optimization. *Inverse Probl Sci Eng* 2018;26(6):792–810.

- [31] Zhang L, Yang G, Hu D, Han X. An approach based on level set method for void identification of continuum structure with time-domain dynamic response. *Appl Math Model* 2019;75:446–80.
- [32] Yoon GH, Kim YY. Element connectivity parameterization for topology optimization of geometrically nonlinear structures. *Int J Solids Struct* 2005;42(7):1983–2009.
- [33] Ester M, Kriegel HP, Sander J, Xu X. A density-based algorithm for discovering clusters in large spatial databases with noise. In: *kdd*, Vol. 96; 1996. p. 226–31.
- [34] Rahai M, Esfandiari A, Bakhshi A. Detection of structural damages by model updating based on singular value decomposition of transfer function subsets. *Struct Control Health Monitor* 2020;27(11):e2622.
- [35] Bendsøe MP. Optimal shape design as a material distribution problem. *Struct Optim* 1989;1:193–202.
- [36] Huang X, Xie Y. Convergent and mesh-independent solutions for the bi-directional evolutionary structural optimization method. *Finite Elements Anal Des* 2007;43(14):1039–49.
- [37] Kammer DC. Sensor placement for on-orbit modal identification and correlation of large space structures. *J Guid, Control, Dynam* 1991;14(2):251–9.
- [38] Gomes GF, da Cunha SS, da Silva Lopes Alexandrino P, Silva de Sousa B, Anceletti AC. Sensor placement optimization applied to laminated composite plates under vibration. *Struct Multidiscip Optim* 2018;58(5): 2099–118.
- [39] Ostachowicz W, Soman R, Malinowski P. Optimization of sensor placement for structural health monitoring: a review. *Struct Health Monitor* 2019;18(3):963–88.
- [40] Qu Z-Q. Adaptive mode superposition and acceleration technique with application to frequency response function and its sensitivity. *Mech Syst Signal Process* 2007;21(1):40–57.
- [41] Saxena A, Prasad M, Gupta A, Bharill N, Patel OP, Tiwari A, Er MJ, Ding W, Lin C-T. A review of clustering techniques and developments. *Neurocomputing* 2017;267:664–81.
- [42] Ezugwu AE, Ikotun AM, Oyelade OO, Abualigah L, Agushaka JO, Eke CI, Akinyelu AA. A comprehensive survey of clustering algorithms: State-of-the-art machine learning applications, taxonomy, challenges, and future research prospects. *Eng Appl Artif Intell* 2022;110:104743.
- [43] Kanagala HK, Krishnaiah VJR. A comparative study of k-means, dbscan and optics. In: 2016 International conference on computer communication and informatics (ICCCI). IEEE; 2016. p. 1–6.
- [44] Murugesan N, Cho I, Tortora C. Benchmarking in cluster analysis: a study on spectral clustering, dbscan, and k-means. In: *Data analysis and rationality in a complex world* 16, Springer; 2021. p. 175–85.
- [45] Svanberg K. The method of moving asymptotes—a new method for structural optimization. *Int J Numer Methods Eng* 1987;24(2):359–73.
- [46] Raich AM, Liszkai TR. Multi-objective optimization of sensor and excitation layouts for frequency response function-based structural damage identification. *Comput-Aided Civil Infrastruct Eng* 2012;27(2):95–117.